

# Constructing Boundary-identical Microstructures by Guided Diffusion for Fast Multiscale Designs

Jingxuan Feng<sup>1+</sup> · Lili Wang<sup>1+</sup> · Xiaoya Zhai<sup>1\*</sup> · Kai Chen<sup>2</sup> · Wenming Wu<sup>3</sup> · Ligang Liu<sup>1</sup> · Xiao-Ming Fu<sup>1\*</sup>

Received: date / Accepted: date

**Abstract** We propose a novel method to construct large-scale boundary-identical microstructure datasets with high attribute coverage for highly efficient multiscale design. Central to our technique is using a deep generative model to generate microstructures under the two conditions, including the specified boundary and homogenized elastic tensor. We achieve the desired dataset by alternately adding microstructures with diverse attributes constructed by the deep generative model into the dataset and retraining the deep generative model. Sixteen compatible metamaterial datasets with high attribute coverage are constructed by our method. We demonstrate the effectiveness and practicability of the obtained datasets over various multiscale design examples. Specifically, in the design of a mechanical cloak, we utilize macrostructures with  $30 \times 30$  elements and microstructures filled with  $256 \times 256$  elements. The entire reverse design process is completed within one minute, significantly enhancing the efficiency of the multiscale optimization.

**Keywords** Multiscale design · Boundary-identical microstructures · Large-scale datasets · High attribute coverage · Self-conditioned diffusion model · Active learning

## 1 Introduction

Advancements in modern manufacturing enable the creation of intricate structures spanning macro- and microscales, known as multiscale structures. These structures provide a sophisticated way to improve performance for specific applications, including lightweight design Orme et al. (2018); Zhang et al. (2020); Park et al. (2005), enhanced strength Hu et al. (2019); Mirzendehtel et al. (2018), superior thermal conductivity Feng et al. (2024); Dirker and Meyer (2013), and other essential attributes Yoon et al. (2020); Im et al. (2003). Diverse methods for designing multiscale structures are comprehensively discussed in Wu et al. (2021). Metamaterials serve as fundamental building blocks of multiscale structures. Mechanical metamaterials, a branch of metamaterials, allow customization of elastic properties by modifying fine-scale structures. These materials, created through periodic or graded arrangements, exhibit unique properties in multiscale structures.

We focus on constructing large-scale metamaterial datasets satisfying the following two requirements. First, geometric connectivity between adjacent metamaterials is crucial for periodic arrangements, influencing the propagation of forces, waves, and other physical phenomena within the material; thus, geometric connectivity must be strictly satisfied for our dataset. Moreover, metamaterials satisfying the geometric connectivity constraints greatly simplify the multi-scale design process, thus significantly improving efficiency. Such geometric connectivity constraints can be enforced using the same boundary and orthogonal symmetry. Besides, we opt for cubic symmetric microstructures for simplicity of calculation. Therefore, the connectivity constraint can be converted to require that the microstructures have (1) the same boundary and (2) cubic symmetry. Second, the dataset is required to be large-scale and achieve high attribute coverage. Such a dataset has at least two ad-

<sup>1</sup>School of Mathematical Sciences, University of Science and Technology of China, Hefei, Anhui 230026, P.R. China

<sup>2</sup>Beijing Academy of Artificial Intelligence, Beijing 100190, P.R. China

<sup>3</sup>Hefei University of Technology, Hefei, Anhui 230026, P.R. China

<sup>+</sup>These authors contributed equally to this work.

\*Corresponding Author. E-mail: xiaoyazhai@ustc.edu.cn (Xiaoya Zhai) E-mail: fuxm@ustc.edu.cn (Xiao-Ming Fu)

vantages in multiscale structural design based on mechanical properties: (1) providing a large and feasible design space and (2) increasing the possibility of alignment with required attributes.

However, generating such a metamaterial dataset is challenging. The reasons are twofold. First, the diversity of generated structures of previous structural optimization algorithms Wang et al. (2016); Zobaer and Sutradhar (2020); Zhao et al. (2023); Schumacher et al. (2015); Cramer et al. (2016); Wang et al. (2017); Garner et al. (2019); Zhai et al. (2024); Du et al. (2018) is poor. Moreover, the hard connectivity constraint further limits the scope of attribute coverage. Second, choosing a boundary for all cubic symmetric structures to realize the goal of high attribute coverage is extremely difficult or clueless.

There are three established methods for generating connectable metamaterials, including parametric modeling Wang et al. (2016); Zobaer and Sutradhar (2020); Zhao et al. (2023), geometric interpolation Schumacher et al. (2015); Cramer et al. (2016); Wang et al. (2017), and connectivity topology optimization Garner et al. (2019); Zhai et al. (2024); Du et al. (2018). In parametric modeling, predefined microstructures require parameter adjustments to meet specific physical property requirements, involving an experiential design process with continuous trial and error. Geometric interpolation necessitates two pre-defined deformed structures and allows for the complete microstructure sequence through non-uniform interpolation. Topology optimization utilizes connectivity as a constraint, employing gradient descent for geometric connectivity between microstructures. However, previous work did not ensure fully identical boundaries. Incomplete boundary connectivity may result in faults and stress concentration at the discontinuities. Moreover, it can lead to complications in subsequent manufacturing processes. Despite ensuring connectivity, each method is limited in generating large-scale microstructure datasets with high attribute coverage.

This paper proposes a novel method to construct large-scale cubic symmetric metamaterial datasets with the same boundary and high attribute coverage. The key to our algorithm is using a deep generative model to achieve diverse microstructures with high attribute coverage under boundary-identical and cubic symmetric constraints. Specifically, we adopt a self-conditioning diffusion model to generate microstructures under two conditions: (1) the specified boundary and (2) the specified homogenized elastic tensor. We can achieve high attribute coverage when the coverage space of specified homogenized elastic tensors is large enough.

Training the self-conditioning diffusion model needs a dataset. However, constructing such a dataset is our goal. Thus, this is a challenging chicken-and-egg problem. To this end, we propose a practical strategy to solve it. First, we train a self-conditioning diffusion model using the ini-

tial microstructure dataset constructed by the optimization algorithm with the cubic symmetric constraint and without the boundary-identical condition. Besides, we cluster the microstructure boundaries to form a small set of seed boundaries. Then, we run the diffusion model for each seed boundary to generate diverse microstructures by specifying various homogenized elastic tensors and fixing the seed boundary. These microstructures form a boundary-identical dataset for each seed boundary. Finally, we obtain the desired dataset by iteratively retraining a diffusion model using each boundary-identical dataset and adding the microstructures constructed by the trained model into the dataset.

As far as we know, we are the first to construct large-scale metamaterial datasets with the same boundary and high attribute coverage. The dataset is inherently conducive to multiscale design and effectively addresses a crucial issue in multi-scale structures - the connectivity problem. We utilize the dataset for two multi-scale design scenarios: a mechanical cloak design and a customized displacement design. Through testing various boundary cases, hole configurations, and cell variations, we demonstrate the feasibility and versatility of the datasets. It is noteworthy that in the design of the mechanical cloak, we employ  $30 \times 30$  macro units and microstructures filled with  $256 \times 256$  elements. The entire reverse design process is accomplished within one minute, markedly enhancing the efficiency of multi-scale optimization (Figure 1). Code for this paper is available at <https://github.com/Schnabel-8/BDR-diffusion>, and the datasets are publicly available at <https://rec.ustc.edu.cn/share/b9e072b0-306a-11ef-91cb-dfb6325d6cc5>.

## 2 Related works

*Connectable microstructures* Three methods - parametric modeling Wang et al. (2016); Zobaer and Sutradhar (2020); Zhao et al. (2023), geometric interpolation Schumacher et al. (2015); Cramer et al. (2016); Wang et al. (2017), and topology optimization Garner et al. (2019); Zhai et al. (2024); Du et al. (2018) - play crucial roles in generating connectable metamaterials. Parametric modeling effectively describes microstructure geometries for design purposes, yet achieving structures meeting specific performance criteria involves a trial-and-error process. Similarly, geometric interpolation ensures microstructural connectivity, but assessing its performance improvement remains challenging. Therefore, these methods are often combined with topology optimization techniques for enhanced results. Zobaer and Sutradhar Zobaer and Sutradhar (2020) introduce an innovative approach using supershape-based parametric modeling Gielis (2003) to ensure smooth connectivity at interfaces. Schumacher et al. Schumacher et al. (2015) achieve connectable metamaterials by interpolating from a

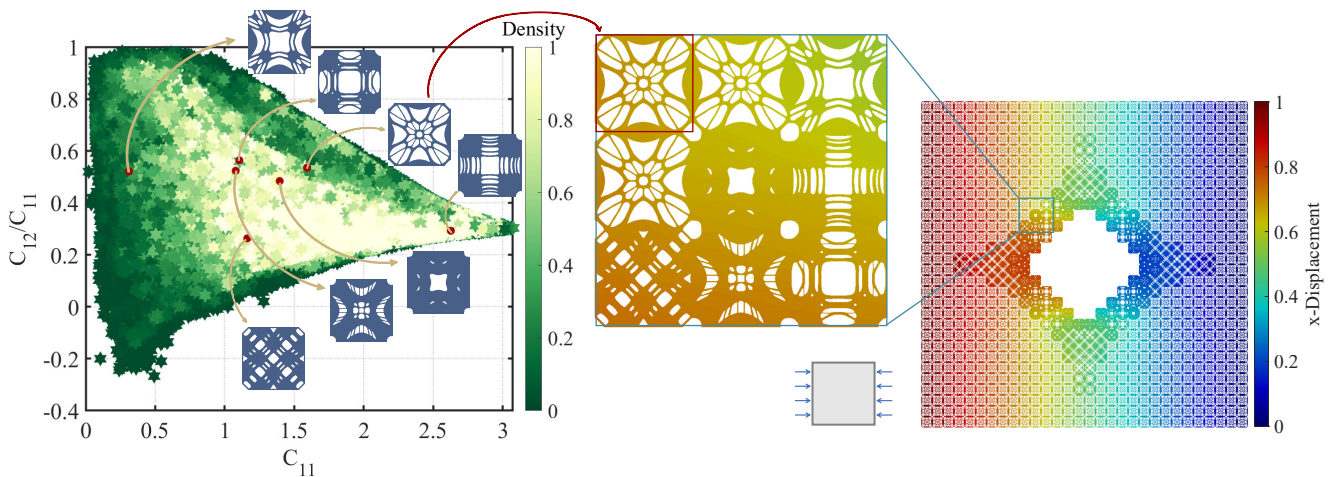


**Fig. 1** Microstructure datasets with identical boundaries (left), along with the mechanical cloak design results derived from the dataset (right).

microstructure database. Shape interpolation methods are developed using signed distance functions or characteristic level set functions Cramer et al. (2016); Wang et al. (2017). Du et al. (2018) combine topology optimization with newly defined connectivity index constraints. Garner et al. (2019) consider geometric connectivity and physical compatibility, reformulating the objective function for the inverse homogenization method. Zhai et al. (2024) propose a differentiable microstructure generation framework, reformulating the problem as a non-uniform heat diffusion process. Despite these advancements, they still need to ensure complete boundary connectivity. Moreover, the initial microstructure will influence the final design, leading to different structures and properties with varied initializations. While all three methods ensure microstructural connectivity, they impose varying limitations on the diversity of the compatibility dataset. Instead, we propose constructing cubic symmetric microstructures with identical boundaries and diverse geometries to ensure complete boundary connectivity.

*Microstructure dataset* Microstructure datasets encompass geometric configurations, physical properties, and performance characteristics. They serve as essential tools for analysis and prediction goals Xu et al. (2021); Chen et al. (2018a); Wang et al. (2021); Peng et al. (2022), experimentation/simulation Steinmetz et al. (2016); Pilchak et al. (2016); Yang et al. (2018); Wang et al. (2022b), and the development of models or algorithms in metamaterial design Wang et al. (2020a); Rade et al. (2021); Ahmad et al. (2022); Patel et al. (2022); Seo and Kapania (2023). Currently, microstructure design-oriented datasets consist primarily of density-based 2D and 3D datasets Wang et al. (2020b); Chan et al. (2021); Lee et al. (2022), along with truss-based datasets Korshunova et al. (2021); Bastek et al. (2022); Zheng et al. (2023a). The construction of metama-

terial datasets is often based on tasks, where factors such as dataset size and attribute coverage can influence the effectiveness of downstream tasks. The methods employed for dataset generation can be broadly categorized into three main types: heuristic generation Chan et al. (2020, 2021); Wang et al. (2023); Zheng et al. (2023a), perturbation generation Lißner and Fritzen (2019); Wang et al. (2020b); Robertson et al. (2023); Lambard et al. (2023), and simulation generation Steinmetz et al. (2016); Yang et al. (2018); Li et al. (2021); Wang et al. (2022a). While shape-driven heuristic methods can generate substantial data rapidly, their inherent lack of control often results in high unpredictability, posing challenges in ensuring dataset quality at the attribute level. Acquiring datasets typically involves extensive experimentation or simulation. However, calculating the effective properties requires numerous finite element simulations, incurring high computational costs and posing challenges in obtaining high-quality datasets. To support multiscale design, a microstructure dataset needs broad attribute coverage, and the geometries should be diverse to ensure compatibility during the filling process.

*AI for microstructures* Neural networks have been successfully used for generating a variety of metamaterials (c.f. the survey in Lee et al. (2023)). Examples include obtaining the homogenization of composite structures Le et al. (2015); Liu et al. (2021); Peng et al. (2022), effective response of stress-strain curves Yuan et al. (2018); Long et al. (2021); Wu et al. (2023); Zheng et al. (2023a), and extreme mechanical metamaterials Wu et al. (2020); Challapalli et al. (2023); Chen et al. (2018a). In terms of performance prediction, AI can establish predictive models by learning from a vast amount of metamaterial data and their corresponding performance characteristics Kautz (2021); Lee et al. (2022); Peng et al. (2022). This enables researchers to rapidly screen potential exceptional metamaterial candidates and save sig-

nificant time in experimentation and simulation. For example, Le et al. (2015) propose a decoupled computation homogenization method for nonlinear elastic materials using neural networks. This method utilizes a neural network model to compute the effective potential. Deng et al. (2022) design a network to predict the nonlinear response curves of hinged quadrilateral metamaterials. Ma et al. (2022) use residual networks instead of finite element analysis to compute strains and successfully employ genetic algorithms for the inverse design of metamaterials with predetermined global strains under magnetic actuation. On the other hand, in the process of inverse design, AI models, particularly generative models, can effectively explore complex design spaces and discover new structures and material combinations that go beyond the limitations of human intuition (Chen et al. (2018b), Zheng et al. (2023a)). Zheng et al. (2023a) utilize a graph-based VAE to design truss structures with customized mechanical properties in both linear and nonlinear states, including designs exhibiting exceptionally stiff, auxetic, pentamode-like, and tailored nonlinear behaviors. Wang et al. (2022a) propose a method using inverse homogenization generative adversarial networks (IH-GANs) for designing variable-density cellular structures. Zheng et al. (2021) develop a GAN-based design method for auxetic metamaterials and successfully use this method to design auxetic metamaterials with predetermined Young’s modulus and Poisson’s ratio. VAEs face challenges in generating high-quality results, often necessitating post-processing. GANs suffer from training difficulties and instability. In contrast, based on a diffusion model, our method offers enhanced stability during training and significantly improved generated quality compared to previous models.

### 3 Dataset Construction

#### 3.1 Overview

*Goals and requirements* Our goal is to construct a large-scale microstructure dataset  $\mathcal{D}$  satisfying the following requirements:

1. Cubic symmetric: each microstructure  $\mathcal{M}$  is cubic symmetric.
2. Identical boundary: the microstructures in the dataset have an identical boundary  $\mathcal{B}$ .
3. High attribute coverage: the physical properties of the microstructures cover a large space  $\mathcal{S}$ .

The first and second requirements are hard constraints to ensure that the microstructures can achieve full compatibility in multiscale design. The third requirement aims to increase the choice space in multiscale design significantly.

*Methodologies* To ensure the diversity of microstructures, we use a deep generative model instead of the optimization methods. Specifically, to reduce the difficulty of meeting the three requirements, we use a self-conditioning diffusion model (Zheng et al. (2023b)) with property guidance, where the properties including the specified boundary  $\mathcal{B}$  and homogenized elastic tensor  $C$  (Section 3.2). Training the self-conditioning diffusion model needs a dataset. Therefore, we develop a practical method to construct an initial dataset  $\mathcal{D}_0$  satisfying the first and second requirements (Section 3.3). Finally, to realize the third requirement, we propose a pipeline based on active learning that alternately runs the following two steps (Figure 2):

1. Training the self-conditioning diffusion model: using the dataset satisfying the first and second requirements to train the self-conditioning diffusion model.
2. Augmenting the dataset: adding the microstructures generated by the self-conditioning diffusion model into the dataset.

#### 3.2 Self-conditioning diffusion model with property guidance

*Diffusion Model* Diffusion models usually denoise a Gaussian noise  $x_T$  towards a data sample  $x_0$  in  $T$  steps, involving both forward and reverse processes during training (Figure 3).

- **Forward Process**: This process begins with a data sample  $x_0$  and progressively generates a noisy sample  $x_t$  at each time step  $t$ . The addition of noise is achieved by sampling a Gaussian noise  $\epsilon \sim \mathcal{N}(0, I)$ .

$$x_t = \sqrt{\gamma_t}x_0 + \sqrt{1 - \gamma_t}\epsilon \quad (1)$$

$\gamma_t$  is a noise schedule that gradually changes from 1 to 0. At each step, the model adds a bit of this Gaussian noise to the data sample, thereby gradually transforming the original data  $x_0$  into a noisy version  $x_t$  over  $T$  steps.

- **Reverse Process**: The reverse process commences from pure Gaussian noise  $x_T \sim \mathcal{N}(0, 1)$ . The model is trained to learn the denoising sequence, effectively reversing the noising process step by step until it reaches  $x_0$ . In each step of this process, the model takes a noisy sample  $x_t$  and estimates the less noisy sample  $x_{t-1}$ . We generally use a neural network to predict this estimation. However, instead of directly learning the transition from  $x_t$  to  $x_{t-1}$ , we employ a network, denoted as  $f(x_t, t)$ , to predict  $x_0$  from  $x_t$ . We then estimate  $x_{t-1}$  based on  $x_t$  and the predicted  $\hat{x}_0$ . Following Ho et al. (2020), the backbone of this denoising network is implemented as a U-Net architecture shown in Figure 3.



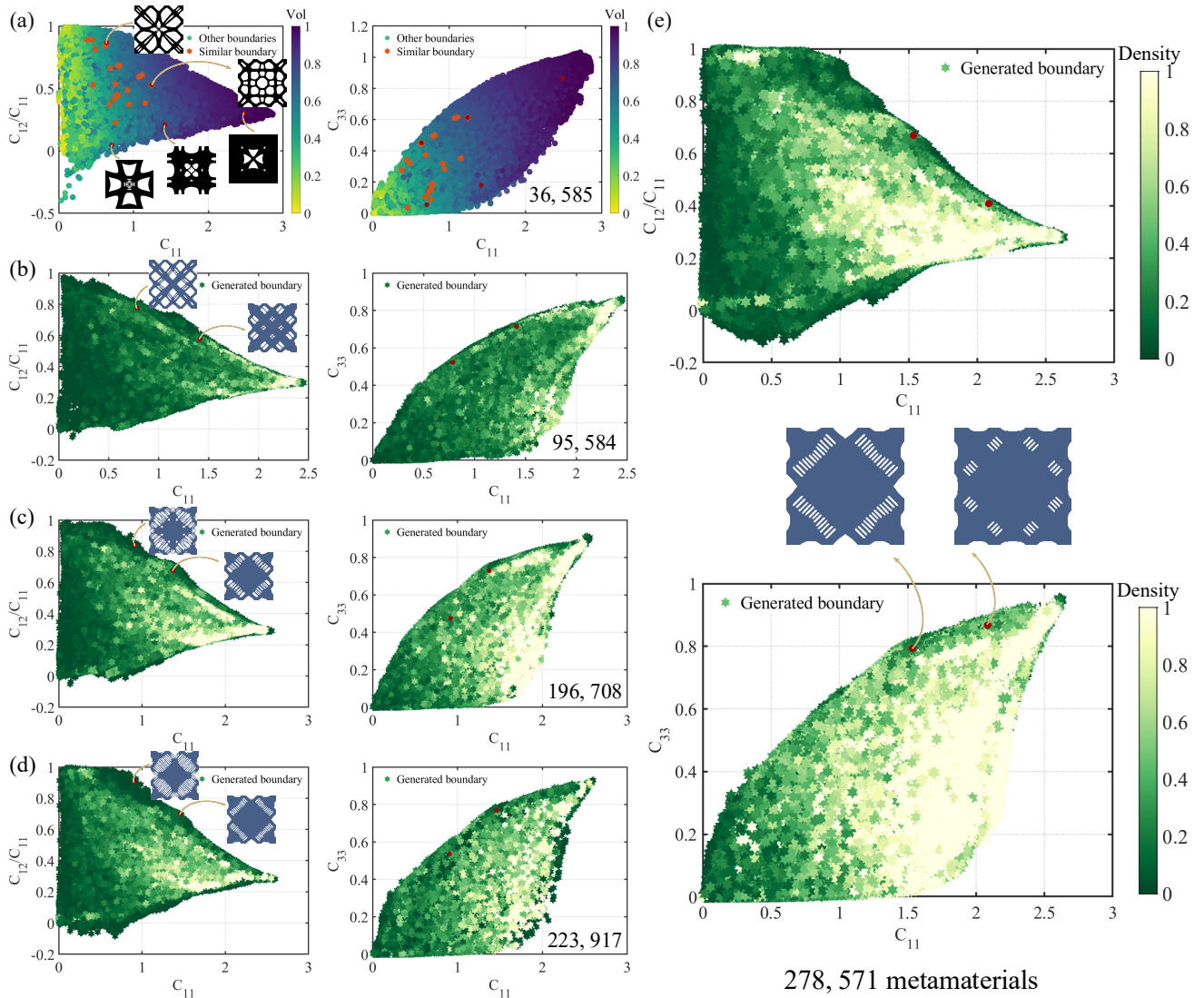


**Fig. 2** Overview of our framework: We initiate the process by training a self-conditioning diffusion model using an initial dataset (a), where microstructures exhibit diverse boundaries. Subsequently, we execute the diffusion model with a single seed boundary, yielding microstructures with varied elastic tensors while maintaining a fixed boundary (b). The resulting microstructure dataset is employed to train a new diffusion model. Through an iterative process (c-d) of generating additional microstructures, incorporating them into the dataset with a consistent boundary, and retraining the diffusion model, we attain the final dataset characterized by a uniform boundary and extensive attribute coverage (e).

*Self-conditioning* Self-conditioning is a technique proposed by Chen et al. (2022) to improve the generation quality of diffusion models. The specific approach is as follows: we consider a slightly different denoising function,  $f(x_t, \hat{x}'_0, t)$ , which takes the concatenation of the previous estimation  $\hat{x}'_0$  for  $x_0$  and  $x_t$  as input to the network. As suggested by Chen et al. (2022), during the training process, we set  $\hat{x}'_0$  to  $f(x_t, 0, t)$  with probability 50%, and at other times,  $\hat{x}'_0$  is set to 0, i.e., without self-conditioning.

*Representations and conditions* We represent each microstructure using a binary matrix of size  $256 \times 256$ , where 0 represents empty space and 1 represents solid space. Since the microstructures we consider are cubic symmetric, we

only utilize the top-left quarter of the microstructure during the training and generation process. Besides, we use symmetric Gaussian noise to ensure that the generated microstructures strictly adhere to cubic symmetry.

Our self-conditioning diffusion model aims to generate microstructures based on the given boundary and elastic tensor. For microstructures with cubic symmetry, their homogenized elastic tensor can be fully determined by three independent components:  $C_{11}$ ,  $C_{12}$ , and  $C_{33}$ . Therefore, we only consider these three components as the conditions for elastic tensor. We incorporate them into the network using classifier-free guidance Ho and Salimans (2021). Here is the specific implementation: We encode  $C_{11}$ ,  $C_{12}$ , and  $C_{33}$  us-

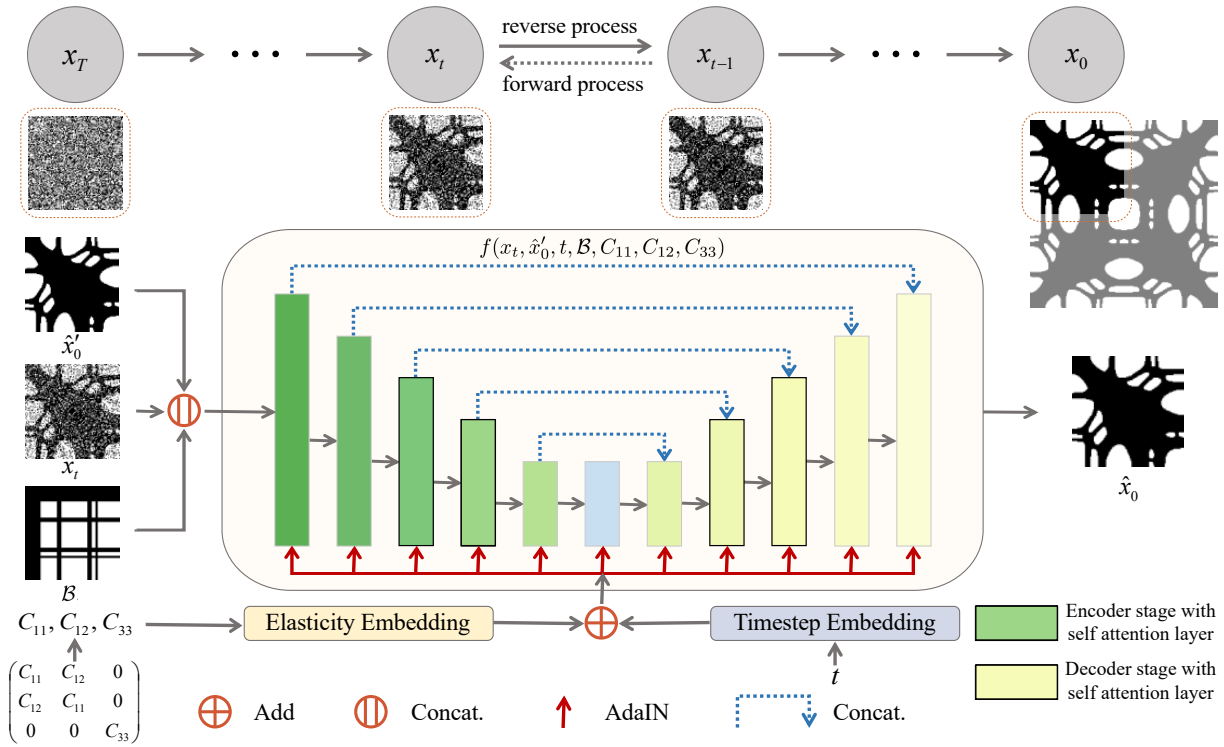


Fig. 3 Network architecture of the proposed self-conditioning diffusion model.

ing learnable sinusoidal embeddings. Then, we add the three encoded vectors with the timestep embedding and incorporate the result into every layer of the U-Net through adaptive instance normalization. According to Ho and Salimans (2021), during training, we randomly set the elastic tensor condition to empty with a probability of 20% and set the guidance scale to 1 during generation.

For the boundary constraint, we encode the boundary information into an image and then append this image to the network’s input. Specifically, assuming that we want to use the boundary  $\mathcal{B}$  of a particular microstructure as a condition, we first extract a  $128 \times 128$  sub-microstructure image from the top-left quarter of the given microstructure and record the positions of the rows and columns where the upper and left boundaries lie. Then, a new binary image is created (default value 0) where the recorded boundary rows and columns are set to 1, establishing a boundary representation for the given microstructure.

*Network architecture* The Encoder and Decoder parts of our U-Net both consist of 5 stages. We set the number of res-blocks for each stage as 1, and channel multiplications for each stage are set to 1, 2, 4, 8, and 8, respectively. Attention resolutions with respect to feature map sizes are set at 4 and 8. The diffusion step number is set to 1,000 with a linear noise schedule during training.

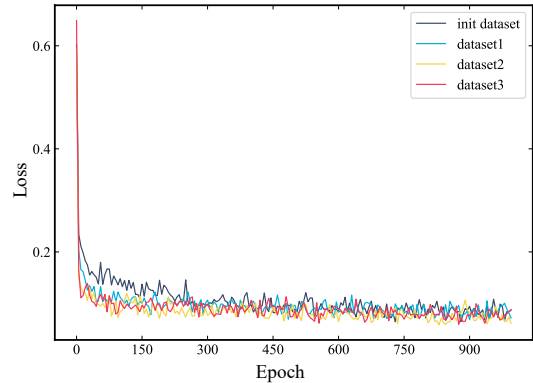
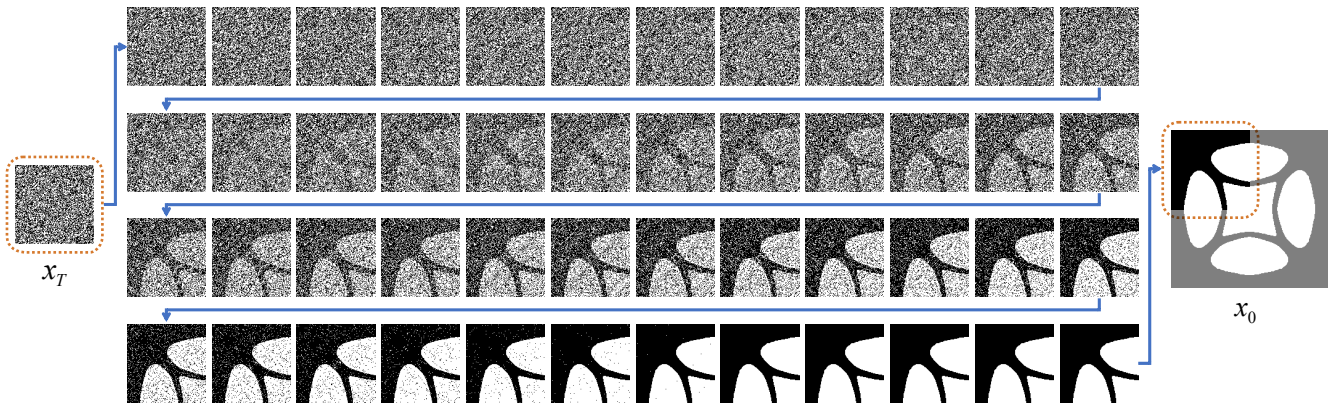


Fig. 4 The training history of the proposed diffusion model on different training sets. Dataset 1, 2, and 3 (Figure 2 (b)-(d)) are three of the intermediate datasets during the iteration process.

*Training details* The network training is based on the following denoising loss:

$$\mathcal{L}_{x_0} = E_{\epsilon \sim \mathcal{N}(0, I), t \sim \mathcal{U}(0, 1)} \|f(x_t, \hat{x}'_0, t, \mathcal{B}, C_{11}, C_{12}, C_{33}) - x_0\|_2^2. \quad (2)$$

We use the AdamW optimizer Kingma and Ba (2014); Loshchilov and Hutter (2017) to train the diffusion model. For each model mentioned below, we fix the learning rate to  $10^{-4}$ , batch size to 256, and train for 1000 epochs. We show the loss function as a function of the iteration number in Figure 4.



**Fig. 5** Complete process for generating microstructures from noise using 50-step DDPM sampling.

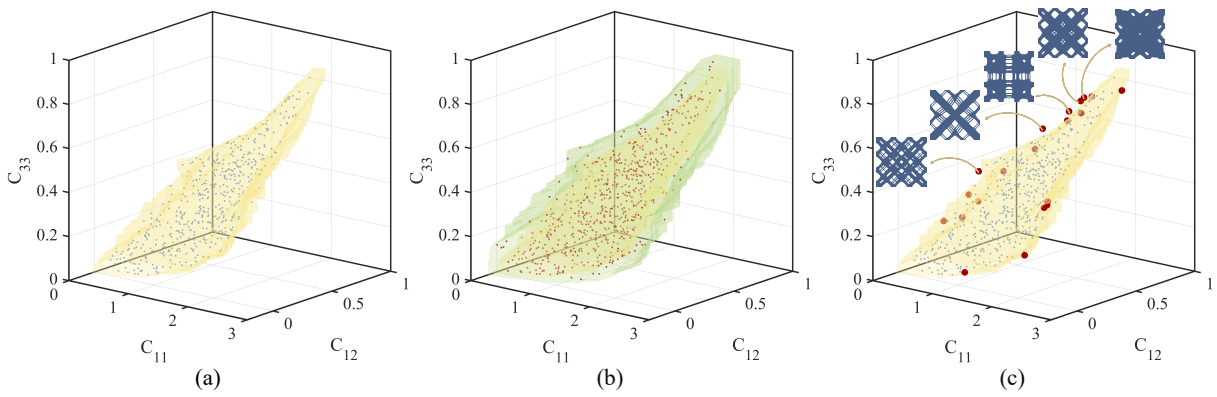


**Fig. 6** Illustration of the generation process: (a) Interior of the Signed Distance Function (SDF) representing the training set's attribute coverage. (b) The expanded SDF (green region) and the target elastic tensor (red points). (c) Microstructures generated by the network that lie beyond the coverage of the training set attributes.

*Generation* We use the diffusion model to generate diverse microstructures under two conditions: (1) the specified boundary and (2) the predefined elastic tensor matrix. To achieve diversity, the elastic tensors should span a large space. To generate elastic tensors that cover a wide and reasonable range, we start by computing the SDF values at each node of a Cartesian grid that encompasses the attribute space of the training dataset Green (2007); Mishchenko (2015), as shown in Figure 6 (a). Then, we set the SDF values to negative for the small neighborhood of nodes where the SDF is less than 0. This ensures that the sampling range is not limited to the coverage range of the training dataset. Finally, we perform sampling in the regions where the SDF is less than 0 to obtain the elastic tensors required for generation. Figure 6(b) displays the expanded range of the SDF and the elastic tensors obtained from the sampling. We input these elastic tensors and the encoding of target boundary together as conditions into the network, and use 50 steps of DDPM sampling for microstructure generation. Figure 6(c) shows some microstructures generated by our generative model that lie outside the attribute space of the training set.

### 3.3 Initializing metamaterial dataset

*Dataset via optimization and perturbation* We use the optimization method Xia and Breitkopf (2015) and shape perturbation to generate a cubic symmetric microstructure dataset  $\hat{\mathcal{D}}$  without identical boundaries and with high attribute coverage:

1. Initializing the dataset: we generate microstructures by optimizing the bulk and shear modulus under various volume fractions. Specifically, we consider a volume fraction range of 0.2 to 0.9 and generate 16,000 distinct microstructures.
2. Perturbing microstructures: utilizing the radial distortion model proposed by Kroon Kroon (2009), each microstructure is subjected to perturbation. For each microstructure, we generate 30 different perturbed versions, resulting in a total of 48,000 perturbed microstructures.
3. Organizing and selecting microstructures: the perturbed microstructures are filtered to retain all fully connected microstructures while discarding the disconnected ones. After filtering, there are about 40,000 microstructures

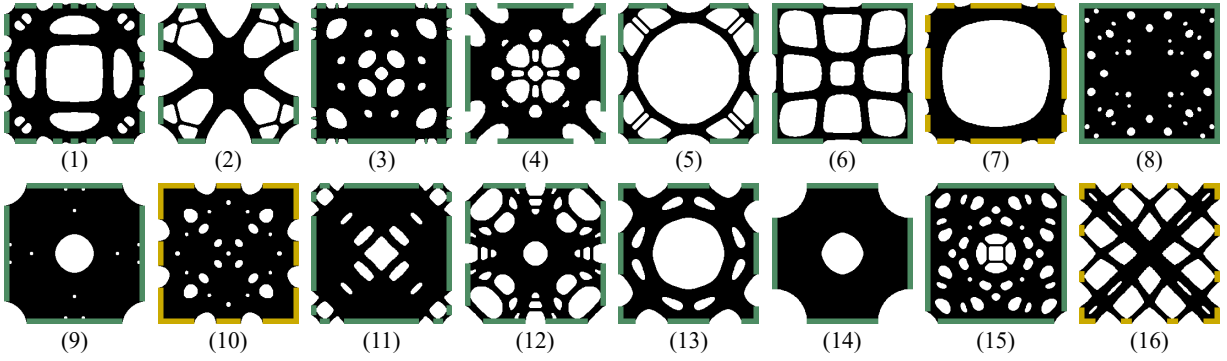


**Fig. 7** Sixteen different boundaries obtained by the clustering method. The boundaries of all microstructures that precisely match the considered boundary are colored green, while the rest are colored yellow.

left. Afterwards, we merge the perturbed microstructures with the optimized microstructures and then remove the geometrically similar structures, and finally obtain a dataset of 36,585 microstructures.

**Boundary Clustering** We perform clustering on the boundaries of microstructures of  $\widehat{\mathcal{D}}$  (Figure 7). Since each microstructure is cubic symmetric, the clustering acts on the boundary of the top-left quarter of the microstructure. Specifically, we use the k-means clustering method to generate a set of seed boundaries  $\{\mathcal{B}_i^{\text{seed}}\}$ . To determine the number of classes, we first select 40 clusters, but the clustering results show several nearly identical boundaries. To address this, we gradually reduce the number of clusters until there are no longer highly similar boundaries in the clustering results. The final cluster number is 24.

**Boundary-constrained generation** Using the dataset, we train a self-conditioning diffusion model  $G$ . For each seed boundary  $\mathcal{B}_i^{\text{seed}}$ , we run the generative model  $G$  to generate various microstructures to form an initial dataset satisfying the boundary-identical and cubic symmetric constraints. Based on the generated results, the initial dataset has limitations regarding its attribute coverage. To this end, we propose our iterative algorithm to alternate model retraining and dataset augmentation.

## 4 Numerical experiments and discussion

All our experiments were done on a server with 2 CPUs (Intel Xeon Silver 4316 2.30GHz), 512GB RAM and 8 Nvidia GeForce RTX 3090 GPUs. The material model has Young’s modulus of  $E = 3$  and Poisson’s ratio of  $\mu = 0.3$ . Linear elements are used to perform finite element analysis.

### 4.1 Network performance analysis

To assess the fidelity of structures generated by our self-conditioning diffusion model in accordance with specified conditions, we executed conditional generation tests on the network trained with the initial dataset. The rationale behind choosing this particular network lies in the diverse array of boundary types present in the initial dataset’s microstructures. This diversity adds complexity to the task of conditional generation, thereby posing a more formidable challenge when utilizing the network trained on the initial dataset as the training set. We designated the boundaries depicted in Figure 1 as the target boundaries for our dataset. Subsequently, we randomly selected 1000 sets of elastic tensors, utilizing the initial dataset’s signed distance function (SDF) as conditions for the generation process. To assess the fidelity of the generated results, we employed homogenization methods to compute their effective properties. Furthermore, we gauged the concordance between the generated elastic tensors and the target elastic tensors using the coefficient of determination ( $R^2$ -score):

$$R^2 = 1 - \frac{\sum_{i=1}^N \|y_i - y'_i\|^2}{\sum_{i=1}^N \|y_i - \bar{y}_i\|^2}, \quad (3)$$

where  $y_i$  denotes the target property ( $C_{11}$ ,  $C_{12}$  or  $C_{33}$ ),  $y'_i$  denotes the actual property of generated microstructures and  $\bar{y}_i$  denotes the mean value of the target property,  $N$  is the number of generated data (1000). The comparative results are shown in Figure 8, revealing that, for each independent component of the elastic tensor considered, the  $R^2$ -score between the generated results and the target consistently surpasses 0.99.

We characterize the microstructure boundaries through a binary vector of length 256. Specifically, for a microstructure represented by a binary matrix, we extract the initial row of the matrix to define the boundary. The  $L_1$  norm is employed to quantify the discrepancy between the generated microstructure boundaries and the designated target



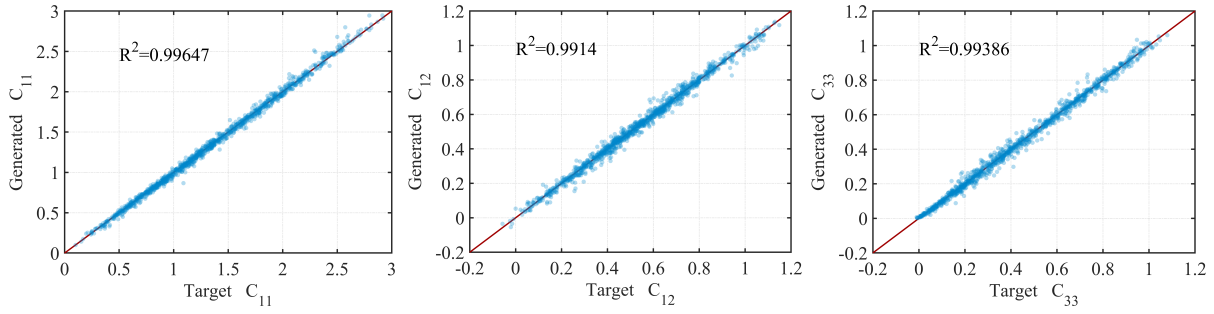


**Fig. 8** The  $R^2$ -score demonstrates the disparity between the attributes of the microstructures generated by the network and the target attributes.

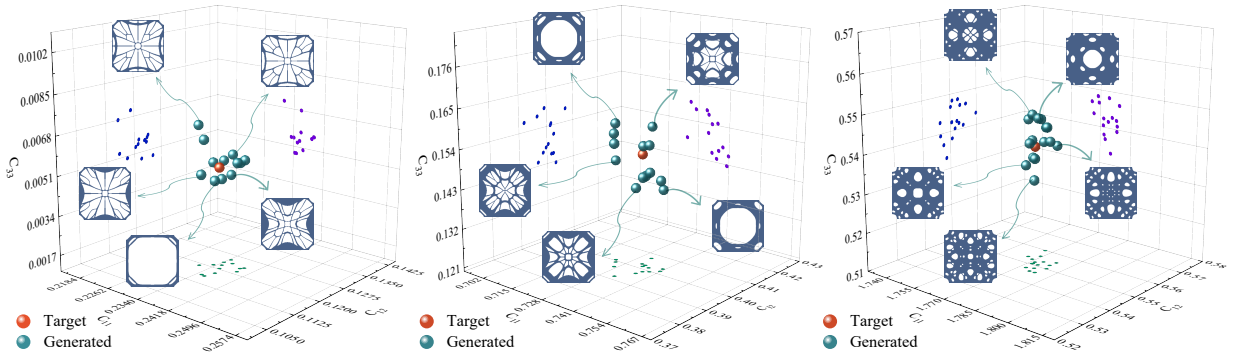


**Fig. 9** The generated results for three different predefined elastic tensors.

boundaries. Following the computation, we determined that all 1000 structures exhibited an effective alignment with the target boundaries, manifesting errors confined within a 2-element range. Moreover, we conducted tests to evaluate the diversity of the network’s generation capabilities. Concretely, we held the boundary conditions constant and selected a target elastic tensor for multiple generations. The generated results under various elastic tensor conditions are depicted in Figure 9. These findings substantiate that our model adeptly captures the one-to-many mapping from attributes to geometry.

#### 4.2 Boundary-identical metamaterials dataset generation

Employing the 24 specified boundary types and elastic tensors generated at random from the signed distance function (SDF) of the initial dataset, we initiate the generation process to acquire an initial dataset characterized by 24 identical boundaries. Upon analyzing the generated results, we observe that 16 of the boundary types shown in Figure 7 exhibit a broad coverage of attributes within the generated dataset. In Figures 1, 2, and 10, we present 16 datasets with identical boundaries and show part of the results that we have constructed. Each dataset consists of more than 100,000 samples. These datasets can be used for subsequent multiscale design or other data-driven research purposes. In Figure 11, we conducted an analysis of the bulk modulus of all microstructures in the aforementioned datasets

and compared them with the Hashin-Shtrikman bound (HS-bound) Hashin and Shtrikman (1963). The structures shown in the figure all achieve 98% or higher of the HS-bound. This indicates that our model has the potential to generate extreme materials with specified boundaries.

#### 4.3 Multiscale metamaterials system design

To demonstrate the approach, we apply the generated boundary-identical metamaterials datasets to design two applications of multiscale metamaterials systems, mechanical cloak design and customized displacement design. For mechanical cloak design, the reference structures (without voids and cloak) are composed of  $30 \times 30$  periodically tessellated base cells chosen in the metamaterials dataset. The reference design space is denoted as  $\Omega$ , and the mechanical cloak is defined in a circle of radius 12 at the center of  $\Omega$  and marked  $\Omega_c$ . The properties of the cloak are evaluated in the remaining areas  $\Omega_s = \Omega/\Omega_c$ , and the stealth capabilities of the cloak are deemed better when the difference between the displacement and the reference displacement is minimized.

As shown in Figure 12 (a), four different boundaries are employed. It is noteworthy that the blue arrow signifies that the designated displacement represents the boundary condition  $u_{bc}$ , while the green arrow indicates that the specified force serves as the boundary condition  $p_{bc}$ . Figure 12 (b) illustrates the relative difference of displacement before and

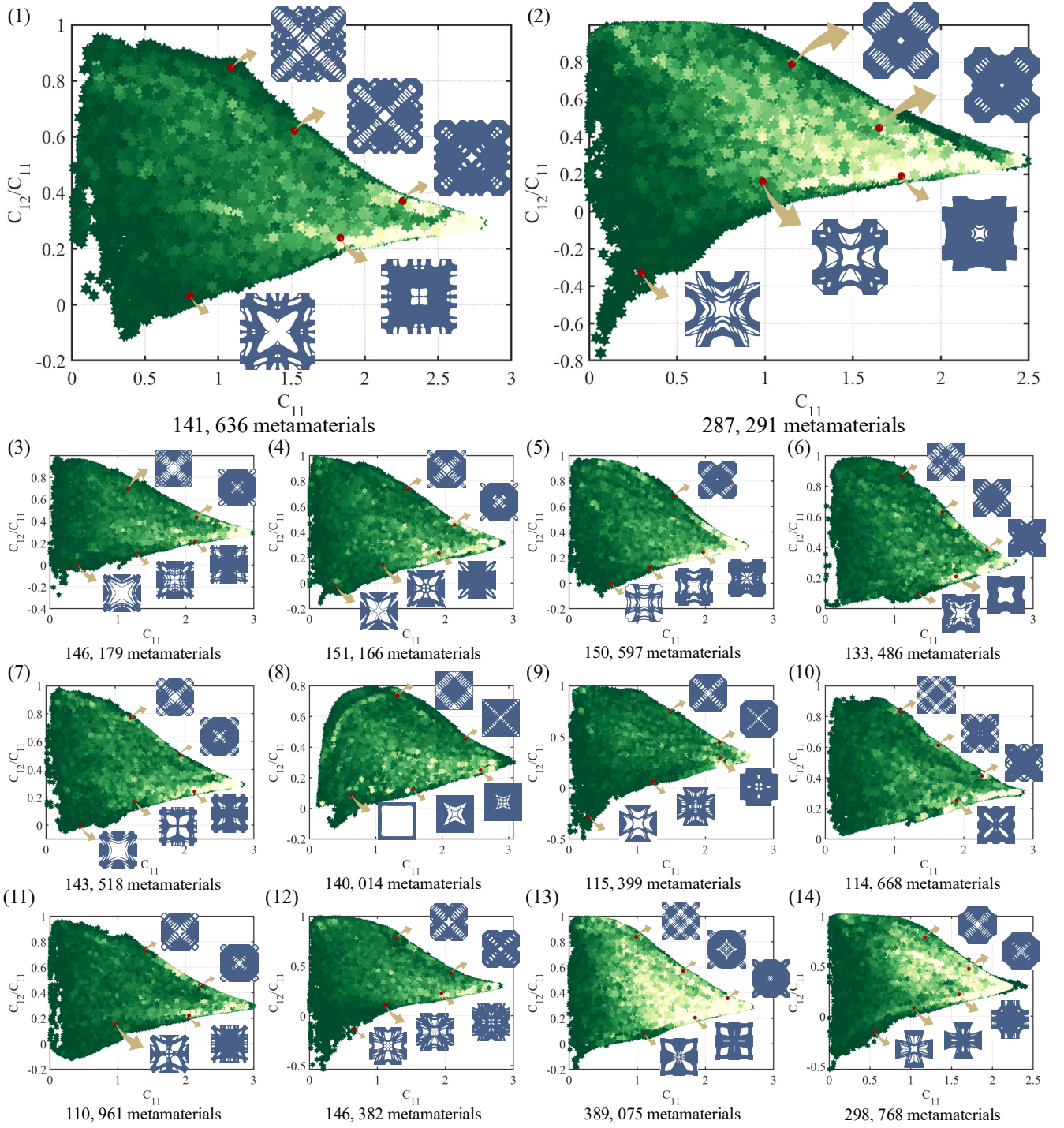


**Fig. 10** The generated 14 large-scale compatible metamaterials datasets.

after the incorporation of the mechanical cloak. For a quantitative measure of the distortion of the displacement field, the relative displacement difference  $\Delta$  is formulated as

$$\Delta = \frac{\sqrt{\sum_{\Omega_s} (\mathbf{u}_c - \mathbf{u}_r)^2}}{\sqrt{\sum_{\Omega_s} (\mathbf{u}_r)^2}}, \quad (4)$$

where  $\mathbf{u}_c$  and  $\mathbf{u}_r$  are the node displacement of mechanical cloak and reference structures. The difference, as indicated by the red bar with the cloak applied, is significantly lower compared to the blue bar without the cloak, especially for the second boundary condition (13.13% vs. 117.40%).

Figure 13 depicts the outcomes of the cloak design for four distinct boundary conditions using the metamaterial



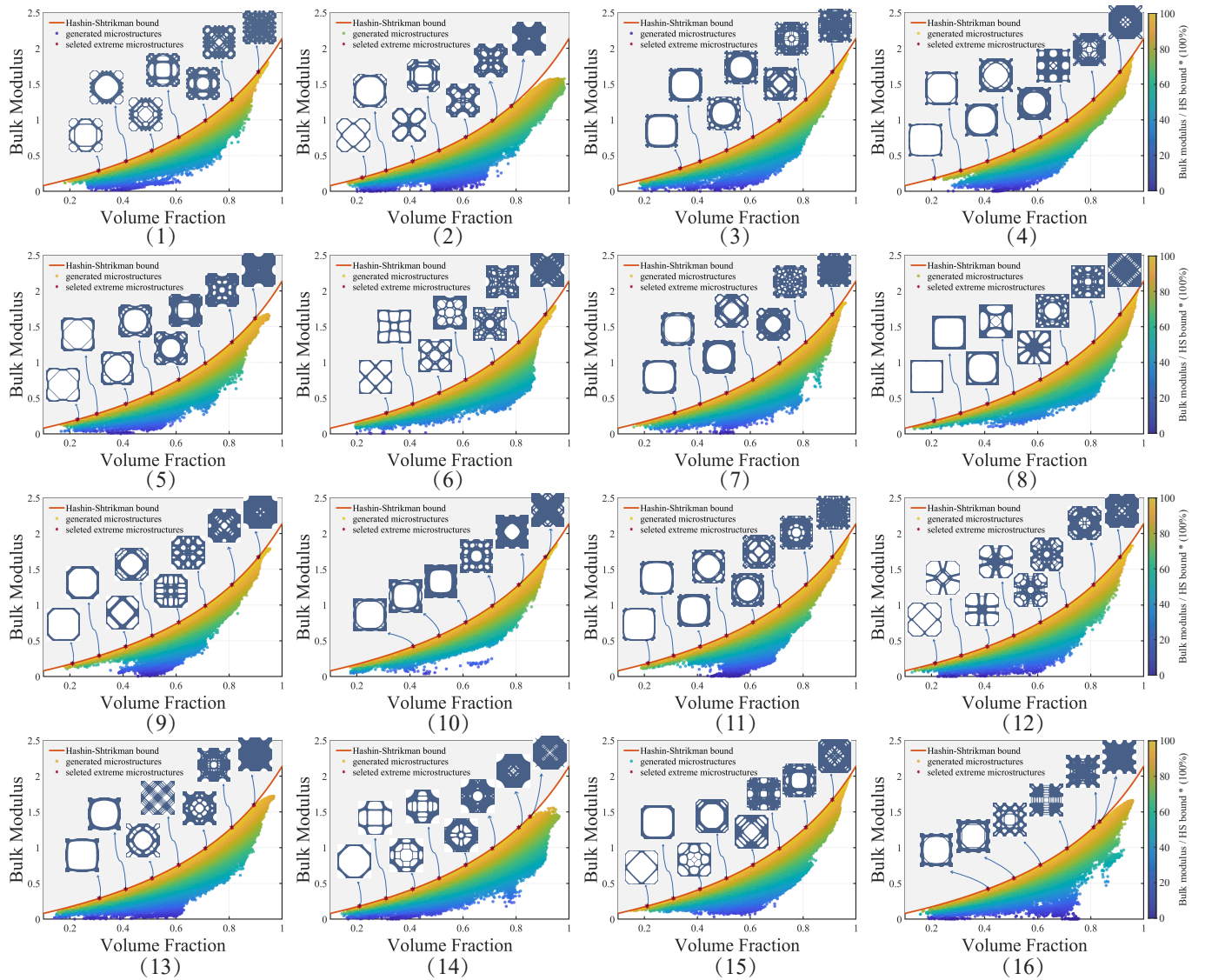


**Fig. 11** The bulk modulus of the microstructures in the 16 datasets. The color bar indicates the proportion of the microstructure's bulk modulus to the corresponding HS-bound. The red line represents HS-bound and the red star represents the selected microstructures that reach 98% HS-bound.

dataset (1) shown in Figure 1. In Figure 13 (b) and (d), it is evident that under the pressure-free and dilating boundary conditions, the displacements in the  $x$  and  $y$  directions in the results without the cloak significantly deviate from those of the reference structures. The addition of the cloak structure notably reduces the displacement gap. The dataset generated by our method shown in Figure 1 is capable of addressing complex deformation scenarios while maintaining full boundary connectivity, resulting in an error reduction of less than 13.2% for the aforementioned four examples.

To validate the design capabilities of mechanical cloaks for additional datasets, we conducted tests on 16 datasets shown in Figure 10 under displacement-free boundary conditions, each featuring a hollow circular hole in the center. The results and statistics are shown in Figure 14 and Fig-

ure 12, respectively. The results obtained from the analysis of 16 datasets revealed a maximum difference of 5.6%. The generated datasets encompass a broad spectrum and has the potential to facilitate the design of mechanical cloaks.

For the second application, two examples, face, and gripper, are designed to show the effect of customized displacement design. For the multi-scale structure design of the face, we opted for a combination of  $10 \times 10$  unit cells and utilized the metamaterial dataset presented in Figure 1 for the selection and assembly of metamaterials. When pressure is applied to both sides of the face, the mouth will exhibit a downward curve, creating the appearance of a smile expression. Likewise, in the gripper design, a grid of  $20 \times 20$  unit cells was chosen, and the metamaterial dataset (5) in Figure 10 served as the metamaterial library for optimal de-

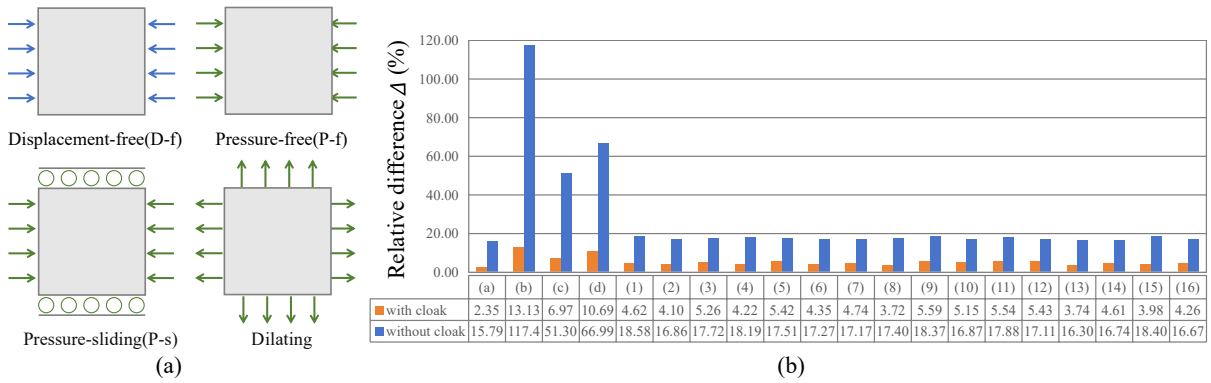


**Fig. 12** (a) Four initial settings (b) Relative displacement differences of cloak design results under different boundary conditions, void shapes and datasets.

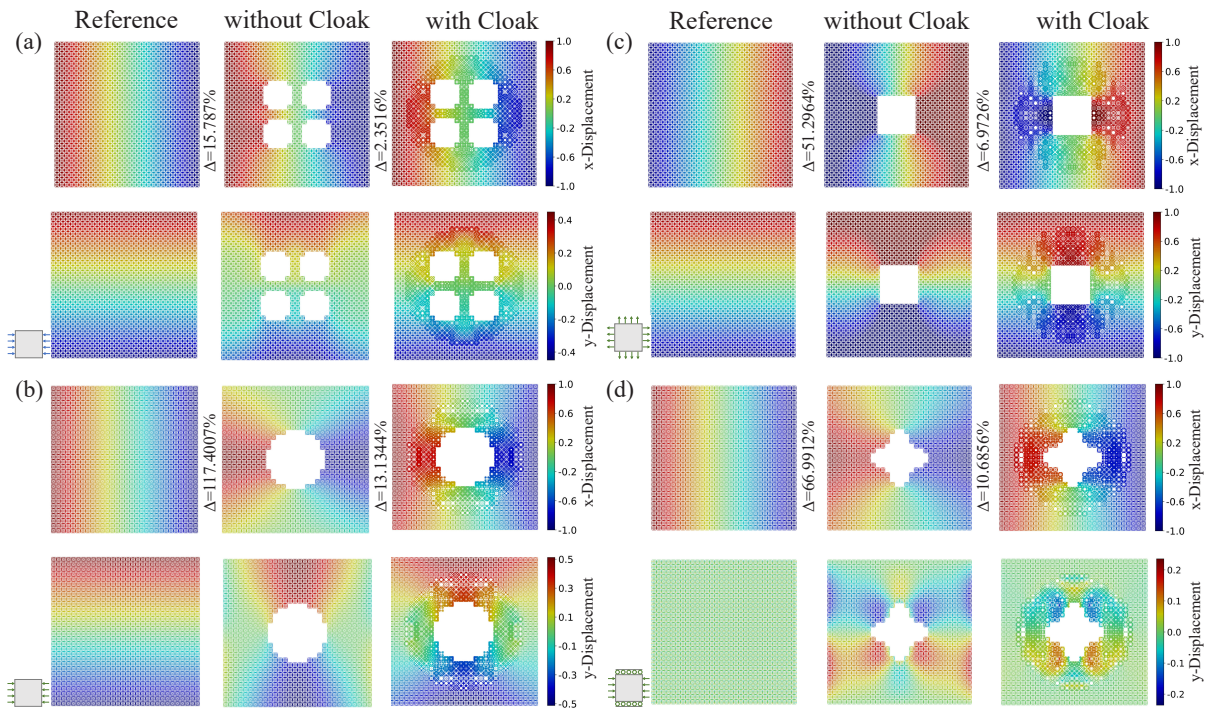


**Fig. 13** Mechanical cloak design results under different boundary conditions and void shapes using metamaterial dataset (1). (a) The results of cloak structure for four circular voids under displacement-free boundary condition (b) The results of cloak structure for circular void under pressure-free boundary condition (c) The results of cloak structure for square void under dilating boundary condition (d) The results of cloak structure for star void under pressure-sliding boundary condition.

sign. When the gripper is compressed vertically on the left side, the structure on the right side contracts towards the central axis. Simulation results indicate that the optimized outcomes align closely with the specified displacement. Applying the calculation formula in Eq. (4), the relative differences for the face and gripper are 12.19% and 8.70%, respectively.

The present study underscores a notable enhancement in the algorithm's efficiency, evidenced by a substantial reduction in the computation time. Specifically, the algorithm has achieved a remarkable improvement, diminishing the orig-

inal calculation time from 10 hours Wang et al. (2020a) to a mere 1 minute. This advancement signifies a notable 600-fold increase in efficiency. In the data-driven approach Wang et al. (2020a) for computing top-down multiscale problems, conducting a single-cell search to ensure connectivity imposes a considerable time burden.

## 5 Conclusion and Future Work

This paper introduces 16 large-scale cubic symmetric microstructure datasets with consistent boundaries and high



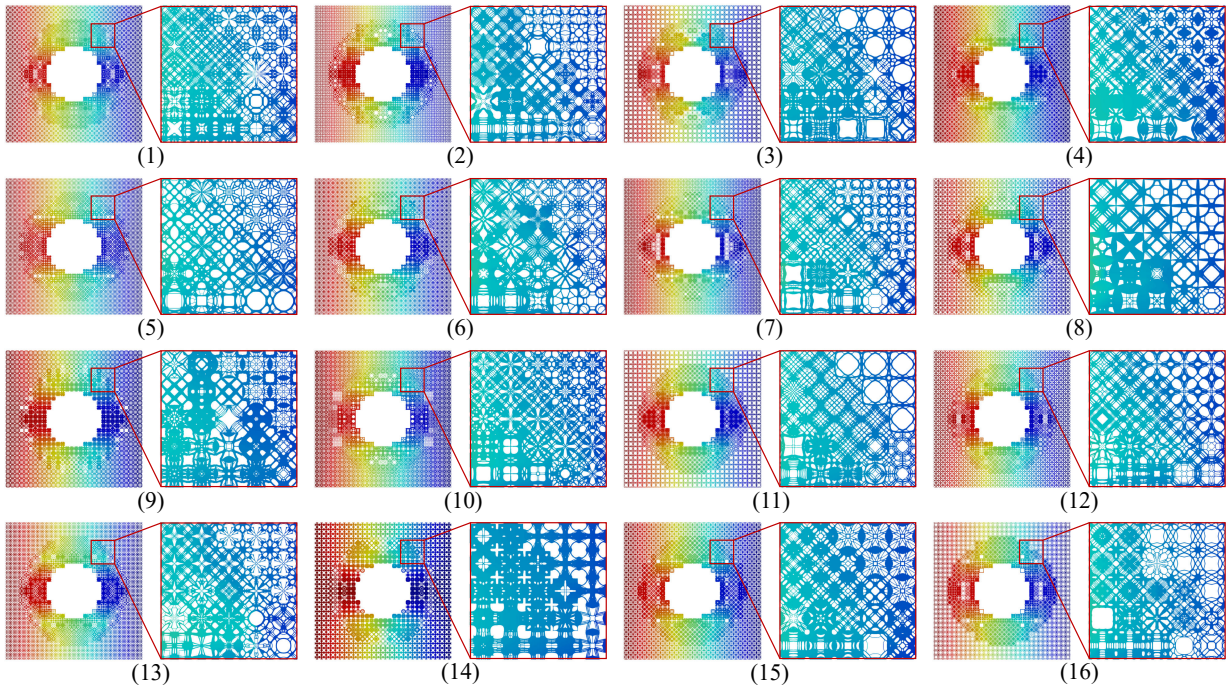


**Fig. 14** Cloak design results under displacement-free boundaries and circular void using 16 different datasets. The red box shows a partial enlargement of the cloak.

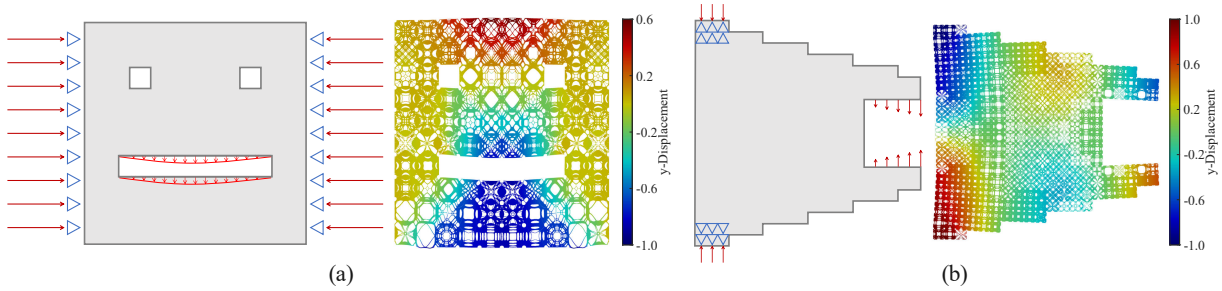


**Fig. 15** The target settings and displacement simulation of optimized results for (a) smiley face filled with  $10 \times 10$  macro unit cells and (b) gripper filled with  $20 \times 20$  macro unit cells.

attribute convergence, generated through a deep generative model. The self-conditioning diffusion model is employed to derive microstructures under two conditions: the specified boundary and the pre-defined homogenized elastic tensor. Initially, inverse homogenization theory is employed to generate the initial dataset. Subsequently, the microstructure boundaries of the dataset are clustered to categorize it into 16 cases. Then, through 16 types of boundary iterations, a series of datasets with a broad range of modulus values and consistent boundaries are generated. We showcase the data generation capabilities of this generative model through the design of two multi-scale structures: mechanical cloaks and structures with specified displacements. By employing numerous examples featuring varying numbers and shapes of voids, diverse boundary conditions, and different base cells, we illustrate that our method excels in multiscale systems. This superiority is validated through numerical simu-

lations and computational efficiency. The proposed datasets are characterized by consistent boundaries, thereby ensuring natural resolution of the connectivity problem. This results in a substantial reduction in calculation time.

Three-dimensional microstructures find more widespread applications, and we intend to explore the extension of the current results to three-dimensional microstructures in future work. This extension poses two potential challenges: (1) The generation of voxel-based 3D microstructure libraries demands significant computational time and memory resources. Balancing generation efficiency with effectiveness becomes a critical consideration. (2) Classifying boundary conditions for 3D microstructures is notably more complex than for their 2D counterparts, which presents a challenging task in determining reasonable boundary categories for 3D microstructures.

**Acknowledgement** This work is supported by the Youth Innovation Key Research Funds for the Central Universities, China (No. YD0010002010), the Open Project Program of the State Key Laboratory of CAD&CG, Zhejiang University (No. A2303).

## Declarations

**Conflict of interest** The authors declare that they have no conflict of interest.

**Replication of results** Code for this paper is available at <https://github.com/Schnabel-8/BDR-diffusion>, and the datasets are publicly available at <https://rec.ustc.edu.cn/share/b9e072b0-306a-11ef-91cb-dfb6325d6cc5>.

## References

- Ahmad W, Wang G, Yan Y (2022) Ann-based inverse goal-oriented design method for targeted final properties of materials. *Applied Sciences* 12(7):3420
- Bastek JH, Kumar S, Telgen B, Glaesener RN, Kochmann DM (2022) Inverting the structure–property map of truss metamaterials by deep learning. *Proceedings of the National Academy of Sciences* 119(1):e2111505119
- Challapalli A, Konlan J, Li G (2023) Inverse machine learning discovered metamaterials with record high recovery stress. *International Journal of Mechanical Sciences* 244:108029
- Chan YC, Ahmed F, Wang L, Chen W (2020) Metaset: An automated data selection method for scalable data-driven design of metamaterials. In: *International Design Engineering Technical Conferences and Computers and Information in Engineering Conference*, American Society of Mechanical Engineers, vol 84003, p V11AT11A021
- Chan YC, Ahmed F, Wang L, Chen W (2021) Metaset: Exploring shape and property spaces for data-driven metamaterials design. *Journal of Mechanical Design* 143(3):031707
- Chen D, Skouras M, Zhu B, Matusik W (2018a) Computational discovery of extremal microstructure families. *Science Advances* 4(1):eaao7005
- Chen D, Skouras M, Zhu B, Matusik W (2018b) Computational discovery of extremal microstructure families. *Science advances* 4(1):eaao7005
- Chen T, Zhang R, Hinton G (2022) Analog bits: Generating discrete data using diffusion models with self-conditioning. *arXiv preprint arXiv:220804202*
- Cramer AD, Challis VJ, Roberts AP (2016) Microstructure interpolation for macroscopic design. *Structural and Multidisciplinary Optimization* 53:489–500
- Deng B, Zareei A, Ding X, Weaver JC, Rycroft CH, Bertoldi K (2022) Inverse design of mechanical metamaterials with target nonlinear response via a neural accelerated evolution strategy. *Advanced Materials* 34(41):2206238
- Dirker J, Meyer JP (2013) Topology optimization for an internal heat-conduction cooling scheme in a square domain for high heat flux applications. *Journal of Heat Transfer* 135(11):111010
- Du Z, Zhou XY, Picelli R, Kim HA (2018) Connecting microstructures for multiscale topology optimization with connectivity index constraints. *Journal of Mechanical Design* 140(11)
- Feng G, Pan G, Feng Y, Zhang X, Qiu L (2024) Topology optimization of controllable porous microstructure with maximum thermal conductivity. *International Journal of Heat and Mass Transfer* 220:124990
- Garner E, Kolken HM, Wang CC, Zadpoor AA, Wu J (2019) Compatibility in microstructural optimization for additive manufacturing. *Additive Manufacturing* 26:65–75
- Gielis J (2003) A generic geometric transformation that unifies a wide range of natural and abstract shapes. *American journal of botany* 90(3):333–338
- Green C (2007) Improved alpha-tested magnification for vector textures and special effects. In: *ACM SIGGRAPH 2007 courses*, pp 9–18
- Hashin Z, Shtrikman S (1963) A variational approach to the theory of the elastic behaviour of multiphase materials. *Journal of the Mechanics and Physics of Solids* 11(2):127–140
- Ho J, Salimans T (2021) Classifier-free diffusion guidance. In: *NeurIPS 2021 Workshop on Deep Generative Models and Downstream Applications*
- Ho J, Jain A, Abbeel P (2020) Denoising diffusion probabilistic models. *Advances in neural information processing systems* 33:6840–6851
- Hu J, Yao S, Gan N, Xiong Y, Chen X (2019) Fracture strength topology optimization of structural specific position using a bi-directional evolutionary structural optimization method. *Engineering Optimization*
- Im CH, Jung HK, Kim YJ (2003) Hybrid genetic algorithm for electromagnetic topology optimization. *IEEE Transactions on Magnetics* 39(5):2163–2169
- Kautz EJ (2021) Predicting material microstructure evolution via data-driven machine learning. *Patterns* 2(7)
- Kingma DP, Ba J (2014) Adam: A method for stochastic optimization. *arXiv preprint arXiv:1412.6980*
- Korshunova N, Papaioannou I, Kollmannsberger S, Straub D, Rank E (2021) Uncertainty quantification of microstructure variability and mechanical behavior of additively manufactured lattice structures. *Computer Methods in Applied Mechanics and Engineering* 385:114049
- Kroon DJ (2009) Pinch and spherize filter. <https://www.mathworks.com/>

- matlabcentral/fileexchange/  
22573-pinch-and-spherize-filter
- Lambard G, Yamazaki K, Demura M (2023) Generation of highly realistic microstructural images of alloys from limited data with a style-based generative adversarial network. *Scientific Reports* 13(1):566
- Le B, Yvonnet J, He QC (2015) Computational homogenization of nonlinear elastic materials using neural networks. *International Journal for Numerical Methods in Engineering* 104(12):1061–1084
- Lee D, Chan YC, Chen WW, Wang L, van Beek A, Chen W (2022) t-metaset: Task-aware acquisition of metamaterial datasets through diversity-based active learning. *Journal of Mechanical Design* 145(3):031704
- Lee D, Chen W, Wang L, Chan YC, Chen W (2023) Data-driven design for metamaterials and multiscale systems: A review. *Advanced Materials* p 2305254
- Li Y, Holmedal B, Liu B, Li H, Zhuang L, Zhang J, Du Q, Xie J (2021) Towards high-throughput microstructure simulation in compositionally complex alloys via machine learning. *Calphad* 72:102231
- Lißner J, Fritzen F (2019) Data-driven microstructure property relations. *Mathematical and Computational Applications* 24(2):57
- Liu X, Tian S, Tao F, Yu W (2021) A review of artificial neural networks in the constitutive modeling of composite materials. *Composites Part B: Engineering* 224:109152
- Long X, Mao M, Lu C, Li R, Jia F (2021) Modeling of heterogeneous materials at high strain rates with machine learning algorithms trained by finite element simulations. *Journal of Micromechanics and Molecular Physics* 6(01):2150001
- Loshchilov I, Hutter F (2017) Decoupled weight decay regularization. *arXiv preprint arXiv:171105101*
- Ma C, Chang Y, Wu S, Zhao RR (2022) Deep learning-accelerated designs of tunable magneto-mechanical metamaterials. *ACS Applied Materials & Interfaces* 14(29):33892–33902
- Mirzendehtdel AM, Rankouhi B, Suresh K (2018) Strength-based topology optimization for anisotropic parts. *Additive Manufacturing* 19:104–113
- Mishchenko Y (2015) A fast algorithm for computation of discrete euclidean distance transform in three or more dimensions on vector processing architectures. *Signal, Image and Video Processing* 9(1):19–27
- Orme M, Madera I, Gschweilt M, Ferrari M (2018) Topology optimization for additive manufacturing as an enabler for light weight flight hardware. *Designs* 2(4):51
- Park KS, Lee JH, Youn SK (2005) Lightweight mirror design method using topology optimization. *Optical engineering* 44(5):053002–053002
- Patel D, Bielecki D, Rai R, Dargush G (2022) Improving connectivity and accelerating multiscale topology optimization using deep neural network techniques. *Structural and Multidisciplinary Optimization* 65(4):126
- Peng H, Liu A, Huang J, Cao L, Liu J, Lu L (2022) Ph-net: Parallelepiped microstructure homogenization via 3d convolutional neural networks. *Additive Manufacturing* 60:103237
- Pilchak AL, Shank J, Tucker JC, Srivatsa S, Fagin PN, Semiatin SL (2016) A dataset for the development, verification, and validation of microstructure-sensitive process models for near-alpha titanium alloys. *Integrating Materials and Manufacturing Innovation* 5:259–276
- Rade J, Balu A, Herron E, Pathak J, Ranade R, Sarkar S, Krishnamurthy A (2021) Algorithmically-consistent deep learning frameworks for structural topology optimization. *Engineering Applications of Artificial Intelligence* 106:104483
- Robertson AE, Kelly C, Buzzy M, Kalidindi SR (2023) Local–global decompositions for conditional microstructure generation. *Acta Materialia* 253:118966
- Schumacher C, Bickel B, Rys J, Marschner S, Daraio C, Gross M (2015) Microstructures to control elasticity in 3d printing. *ACM Trans Graph* 34(4)
- Seo J, Kapania RK (2023) Development of deep convolutional neural network for structural topology optimization. *AIAA Journal* 61(3):1366–1379
- Steinmetz P, Yabansu YC, Hötzer J, Jainta M, Nestler B, Kalidindi SR (2016) Analytics for microstructure datasets produced by phase-field simulations. *Acta Materialia* 103:192–203
- Wang J, Chen WW, Da D, Fuge M, Rai R (2022a) Ih-gan: A conditional generative model for implicit surface-based inverse design of cellular structures. *Computer Methods in Applied Mechanics and Engineering* 396:115060
- Wang J, Zhu S, Chen L, Liu T, Liu H, Lv Z, Wang B, Tan X (2023) Data mining from a hierarchical dataset for mechanical metamaterials composed of curved-sides triangles. *Composite Structures* 319:117153
- Wang L, Chan YC, Ahmed F, Liu Z, Zhu P, Chen W (2020a) Deep generative modeling for mechanistic-based learning and design of metamaterial systems. *Computer Methods in Applied Mechanics and Engineering* 372:113377
- Wang L, Chan YC, Liu Z, Zhu P, Chen W (2020b) Data-driven metamaterial design with laplace-beltrami spectrum as “shape-dna”. *Structural and multidisciplinary optimization* 61:2613–2628
- Wang L, Tao S, Zhu P, Chen W (2021) Data-driven topology optimization with multiclass microstructures using latent variable gaussian process. *Journal of Mechanical Design* 143(3):031708
- Wang L, Boddapati J, Liu K, Zhu P, Daraio C, Chen W (2022b) Mechanical cloak via data-driven aperiodic metamaterial design. *Proceedings of the National Academy of Sciences* 119(13):e2122185119

- Wang Y, Wang L, Ma Zd, Wang T (2016) Parametric analysis of a cylindrical negative poisson's ratio structure. *Smart Materials and Structures* 25(3):035038
- Wang Y, Chen F, Wang MY (2017) Concurrent design with connectable graded microstructures. *Computer Methods in Applied Mechanics and Engineering* 317:84–101
- Wu J, Sigmund O, Groen JP (2021) Topology optimization of multi-scale structures: a review. *Structural and Multidisciplinary Optimization* 63:1455–1480
- Wu L, Liu L, Wang Y, Zhai Z, Zhuang H, Krishnaraju D, Wang Q, Jiang H (2020) A machine learning-based method to design modular metamaterials. *Extreme Mechanics Letters* 36:100657
- Wu Y, Yu W, Shen S (2023) Developing a variable charge potential for hf/nb/ta/ti/zr/o system via machine learning global optimization. *Materials & Design* 230:111999
- Xia L, Breitkopf P (2015) Design of materials using topology optimization and energy-based homogenization approach in matlab. *Structural and multidisciplinary optimization* 52(6):1229–1241
- Xu Y, Weng H, Ju X, Ruan H, Chen J, Nan C, Guo J, Liang L (2021) A method for predicting mechanical properties of composite microstructure with reduced dataset based on transfer learning. *Composite Structures* 275:114444
- Yang Z, Yabansu YC, Al-Bahrani R, Liao Wk, Choudhary AN, Kalidindi SR, Agrawal A (2018) Deep learning approaches for mining structure-property linkages in high contrast composites from simulation datasets. *Computational Materials Science* 151:278–287
- Yoon WU, Park JH, Lee JS, Kim YY (2020) Topology optimization design for total sound absorption in porous media. *Computer Methods in Applied Mechanics and Engineering* 360:112723
- Yuan M, Paradiso S, Meredig B, Niezgodá SR (2018) Machine learning-based reduce order crystal plasticity modeling for icme applications. *Integrating Materials and Manufacturing Innovation* 7:214–230
- Zhai X, Wang W, Chen F, Wu J (2024) Topology optimization of differentiable microstructures. *Computer Methods in Applied Mechanics and Engineering* 418:116530
- Zhang L, Song B, Fu J, Wei S, Yang L, Yan C, Li H, Gao L, Shi Y (2020) Topology-optimized lattice structures with simultaneously high stiffness and light weight fabricated by selective laser melting: Design, manufacturing and characterization. *Journal of Manufacturing Processes* 56:1166–1177
- Zhao Y, Wang Y, Hao J, Wang Y, Wang K, Tai S (2023) Study on mechanical properties of cellular structures with negative poisson's ratio based on the development of abaqus plug-in tool. *Composite Structures* 322:117348
- Zheng L, Karapiperis K, Kumar S, Kochmann DM (2023a) Unifying the design space and optimizing linear and non-linear truss metamaterials by generative modeling. *Nature Communications* 14(1):7563
- Zheng X, Chen TT, Guo X, Samitsu S, Watanabe I (2021) Controllable inverse design of auxetic metamaterials using deep learning. *Materials & Design* 211:110178
- Zheng XY, Pan H, Wang PS, Tong X, Liu Y, Shum HY (2023b) Locally attentional sdf diffusion for controllable 3d shape generation. *ACM Transactions on Graphics (SIGGRAPH)* 42(4)
- Zobaer ST, Sutradhar A (2020) An energy-based method for interface connectivity of incompatible microstructures through parametric modeling. *Computer Methods in Applied Mechanics and Engineering* 370:113278